Available online at www.sciencedirect.com
ScienceDirect
Geochimica et Cosmochimica Acta 73 (2009) 5778–5792
Geochimica et Cosmochimica Acta
www.elsevier.com/locate/gca

Experimental constraints on Pt, Pd and Au partitioning and fractionation in silicate melt–sulfide–oxide–aqueous fluid systems at 800 °C, 150 MPa and variable sulfur fugacity

Aaron S. Bell [a,*], Adam Simon [a], Marcel Guillong [b]

[a] Department of Geoscience and High Pressure Science and Engineering Center, University of Nevada Las Vegas, 4505 Maryland Pkwy, Las Vegas, NV 89154-4010, USA
[b] ETH Institute for Isotopengeologie/Mineral.Rohstoffe, Clausiusstrasse 25, Zürich CH 9082, Switzerland

Received 20 January 2009; accepted in revised form 25 June 2009; available online 19 July 2009

Abstract

We have performed experiments to constrain the effect of sulfur fugacity (fS_2) and sulfide saturation on the fractionation and partitioning behavior of Pt, Pd and Au in a silicate melt–sulfide crystal/melt–oxide–supercritical aqueous fluid phase–Pt–Pd–Au system. Experiments were performed at 800 °C, 150 MPa, with oxygen fugacity (fO_2) fixed at approximately the nickel–nickel oxide buffer (NNO). Sulfur fugacity in the experiments was varied five orders of magnitude from approximately $\log fS_2 = 0$ to $\log fS_2 = -5$ by using two different sulfide phase assemblages. Assemblage one consisted initially of chalcopyrite plus pyrrhotite and assemblage two was loaded with chalcopyrite plus bornite. At run conditions pyrrhotite transformed compositionally to monosulfide solid solution (mss), chalcopyrite to intermediate solid solution (iss), and in assemblage two chalcopyrite and bornite formed a sulfide melt. Run-product silicate glass (i.e., quenched silicate melt) and crystalline materials were analyzed by using both electron probe microanalysis and laser ablation inductively coupled plasma mass spectrometry. The measured concentrations of Pt, Pd and Au in quenched silicate melt in runs with $\log fS_2$ values ranging from approximately 0.0 to −5.0 do not exhibit any apparent dependence on fS_2. The measured Pt, Pd and Au concentrations in mss do vary as a function of fS_2. The measured Pt, Pd and Au concentrations in iss do not appear dependent on fS_2. The data suggest that fS_2, working in concert with fO_2, via the determinant role that these variables play in controlling the magmatic sulfide phase assemblage and the solubility of Pt, Pd and Au as lattice bound components in magmatic sulfide phases, is a controlling factor on the budgets of Pt, Pd and Au during the evolution of magmatic systems.

1. INTRODUCTION

Quantitative constraints on the geochemical behavior of precious and base metals in silicate melt–aqueous volatile phase(s) systems are intrinsically valuable in elucidating the redistribution of metallic, siderophile and chalcophile elements during the evolution of ore-forming magmatic systems. Metallically fertile magmas are a necessary, albeit not sufficient, condition for the formation of magmatic ore deposits. Magmatic differentiation processes play the critically instrumental role in amplifying, by orders of magnitude, the low abundance of most ore metals in crustal reservoirs (cf., Rudnick and Gao, 2003) to ore-grade concentrations. Understanding the character of these processes is critical to the development of predictive models for ore deposit formation. The partitioning of the platinum group elements (PGE) and base metals has been investigated in natural and experimental assemblages in broadly mafic systems, defined as silicate melt coexisting with immiscible Fe–Ni–sulfide melt and/or crystals. Such studies have yielded both empirically estimated and experimentally determined partition coefficient values for the PGE and

* Corresponding author. Tel.: +1 702 895 3573.
E-mail address: bella19@unlv.nevada.edu (A.S. Bell).

0016-7037/$ - see front matter © 2009 Elsevier Ltd. All rights reserved.
doi:10.1016/j.gca.2009.06.037

other metals between co-existing sulfide crystals and/or liquid and silicate liquid, defined as $D_{PGE}^{sul/sil}$.

Published $D_{PGE}^{sul/sil}$ values for the entire group of platinoids range from 10^3 to 10^5 (Fleet et al., 1991; Peach et al., 1990; Stone et al., 1990; Peach et al., 1994; Fleet et al., 1999), consistent with the long recognized enrichment and association of the PGE with sulfide phases in layered-mafic-intrusion-hosted PGE–Ni–Cu deposits.

Significant effort, and concomitant controversy, has been aimed at quantifying the solubility and oxidation state of many noble and base metals in silicate melts. Experimental studies aimed at elucidating noble metal solubilities in Fe-free, mafic-analog silicate melts have demonstrated consistently that PGE concentrations at metal saturation vary proportionally with the oxygen fugacity (fO_2) imposed upon the system (Ertel et al., 1999). Laboratory studies have demonstrated that Pt solubility in melts ranging from basalt to rhyolite, excluding high Ca melts, is less than 1 μg/g at redox conditions (log $fO_2 \leqslant$ NNO) approximating those present in most natural magmatic systems (Borisov and Palme, 1997; Ertel et al., 1999; Farges et al., 1999; Blaine et al., 2005). In addition to the dependence of PGE solubility on fO_2, it is likely that PGE solubilities are dependent on sulfur fugacity (fS_2). Jugo et al. (1999) hypothesized that fS_2 is important in controlling the solubility of Cu and Au in sulfide phases during the evolution of magmatic systems. While their experimental study was performed at a single fO_2 (NNO + 0.5) and fS_2 (log $fS_2 = -1$) condition, they hypothesized that fS_2 may control the partitioning of Au between silicate melt and sulfide, in this case pyrrhotite (po), by one possible equilibrium such as

$$\mu_{AuO_{0.5}}^{melt} + \mu_{FeS}^{po} + 0.5\mu_{S_2}^{sys} = \mu_{AuFeS_2}^{po} + 0.25\mu_{O_2}^{sys} \quad (1)$$

where μ_i^j is the chemical potential of component i in phase j. Eq. (1) suggests that variation in fS_2 and fO_2, owing to processes such assimilation of country rock (i.e., introduction of reduced and/or oxidized sulfur) and degassing, and associated auto-oxidation of the magma (cf., Candela, 1991), may play a determining role in the metal enrichment process of the evolving magmatic system. For example, assimilation of reduced country rock will drive the magma toward lower fS_2, hence favoring the mass transfer of ore metals from the silicate melt into sulfide (e.g., Au into sulfide as written in Eq. (1)). Fractionation and subsequent removal of sulfide phases at depth during ascent of the magma will reduce the potential for metals to be later scavenged and redistributed by magma-evolved aqueous fluids.

In this study we investigated the role of fS_2 on the solubilities of Pt, Pd, Au and Cu in an H_2O-saturated rhyolite silicate melt, sulfide and oxide phase system at 800 °C and 150 MPa. Sulfur fugacity was controlled by using different sulfide phase assemblages to impose fS_2 that span the range of fS_2 values found in many natural systems. The results demonstrate that changes in fS_2 of an evolving sulfide-saturated magma shift the stable phase assemblage to an assemblage with a different capacity to sequester metals. Such chemical changes affect the inherently finite metal budget of the system and have important consequences for the metals available for transport during sulfide fractionation and/or magmatic degassing at the level of ore deposit formation.

2. PROCEDURES

2.1. Starting materials

Starting materials utilized in this study were a synthetic Corning haplogranite glass (provided by Dr. David London, University of Oklahoma), natural hexagonal pyrrhotite (po), bornite (bn), and chalcopyrite (ccp; provided by Dr. George Harlow, American Museum of Natural History), Calumet magnetite (mt; Calumet Skarn, Colorado), and 10 wt.% NaCl eq. NaCl–KCl ± HCl aqueous solutions. The composition of the starting rhyolite glass is provided in Table 1. The starting sulfide phases and mt were characterized by using electron probe microanalysis (EPMA) for major and most of the minor elements and laser ablation inductively coupled plasma mass spectrometry (LA-ICP-MS) for Pt, Pd and Au. The concentration of these elements is less than 1 μg/g in all phases. Small aliquots of Pt and Pd metal foil were added to serve as the Pt and Pd metal sources. Phase relations for the NaCl–KCl–H_2O system indicate that the aqueous fluid at run conditions exists as a one-phase supercritical aqueous fluid (Bodnar et al., 1985; Chou et al., 1992).

2.2. Experimental design

Experiments were performed at 800 °C and 150 MPa in René-41 cold seal pressure vessels. Rhyolite glass, sulfide phases, mt and aqueous solution were loaded (Table 2) into Au capsules (5 mm OD × 2.5 cm length with a 0.2 mm wall thickness) and sealed with a carbon electrode arc welder. Three different assemblages were loaded as follows: Assemblage 1 initially contained cp + po + mt + glass + aqueous fluid, the latter had an initial ratio of NaCl–KCl–HCl of unity. Assemblage 2 contained cp + po + mt + glass + aqueous fluid, the latter had an initial NaCl–KCl ratio of unity and no HCl. Assemblage 3 contained cp + bn + mt + glass + aqueous fluid, the latter had an initial ratio of NaCl–KCl–HCl of unity. At run conditions cp and po in assemblages 1 and 2 transformed to iss and mss; assemblage 3 is interpreted to have contained a sulfide liquid formed from the reaction of bn and cp. Table 2

Table 1
Haplogranite glass composition.

Oxide constituent	wt.%[a]
SiO_2	77.68
TiO_2	0.01
Al_2O_3	12.7
Fe_2O_3	0.28
Na_2O	4.49
K_2O	4.5
Total	99.66

[a] Analyzed by ICP, EPMA and LA-ICP-MS.

Table 2
Summary of all experimental assemblages at run conditions. All starting solutions had a NaCl/KCl ratio of unity.

Assemblage	Run nos.	Phases at run conditions	NaCl/HCl[a]	P (MPa)	T (°C)	$\log_{10} fO_2$	$\log_{10} fS_2$[b]
One	12, 13, 15	iss + mss + mt + rhyolite melt + aqueous supercritical fluid + Pt + Pd + Au	1	150	800	~NNO	−0.19 (0.29)
Two	46, 47, 48, 49, 50	iss + mss + mt + rhyolite melt + aqueous supercritical fluid + Pt + Pd + Au	0	150	800	~NNO	−0.73 (0.11)
Three	32, 33, 34	Intergrown bn and iss + mt + rhyolite melt + aqueous supercritical fluid + Pt + Pd + Au	1	150	800	~NNO	−5.16 (NA)

[a] This is the starting NaCl/HCl ratio of the aqueous fluid.
[b] Nominal sulfur fugacity values are reported as averages calculated with the Toulmin and Barton (1964) algorithm with 1σ errors and should be considered estimates for a given set of experimental runs. See text in Section 2.3 sulfur and oxygen fugacities for a discussion of calculation and interpretation of the experimental meaning of these values.

provides the details of each assemblage. Water was used as the pressure medium. The fO_2 of each experiment was buffered at approximately Ni–NiO by relying on the intrinsic buffering capacity of the René-41 pressure vessels (cf., Chou, 1987). The fO_2 buffering capacity of the vessel has been evaluated by using external Au capsules loaded with Ni and NiO to verify the stability of both phases over run times exceeding 1000 h. Temperature was monitored with factory-calibrated Omega type K (Chromel–Alumel) thermocouples. Run pressure was monitored with a bourdon tube pressure gauge which was calibrated against a factory-calibrated Heise gauge. Thermal gradients in the pressure vessels are 5–7 °C over the length of the experimental capsule. Experimental run duration was varied from 67 to 672 h; run times are provided in Table 3. Experiments were terminated by a nearly isobaric quench in a stream of compressed air from 800 to 200 °C and then immersed in an ambient temperature water bath. Capsules were removed from the vessels, cleaned with lab-grade H_2O, examined optically and weighed to determine if the capsules remained sealed during the experiment. Only capsules that exhibited mechanical integrity, evinced a mass change of $\leqslant 0.3$ mg, and yielded a strong hiss when pierced with a hypodermic syringe, evincing high internal capsule pressure, were processed for analysis.

2.3. Sulfur and oxygen fugacity

Two different starting sulfide phase assemblages were used in an attempt to control fS_2 at a fixed fO_2. The starting sulfide assemblages were po plus cp in assemblages 1 and 2, and cp + bn in assemblage 3. Despite the interdependent nature of the equilibria controlling fO_2 and fS_2, it is routinely assumed that the vastly greater buffering capacity of the Ni-rich pressure vessel fixes the fO_2 (cf. Chou, 1987) of the experimental assemblage via the equilibrium, in the case of po and mt,

$$6FeS^{po} + 4O_2^{sys} = 2Fe_3O_4^{mt} + 3S_2^{mvp} \quad (2)$$

In the absence of large quantities of sulfide, the fO_2 imposed by the vessel in conjunction with the water pressure medium will fix the fH_2 imposed on the experimental system, thus the vessel-controlled fH_2 imposed on the experimental system controls fS_2 via the equilibrium in Eq. (2). As a consequence of fixing fH_2 and fS_2, the fH_2S of the experimental system must also be fixed by the equilibrium

$$H_2 + 1/2S_2 = H_2S. \quad (3)$$

We hypothesize that the progressive sulfidation of the Pt metal chip, added as the Pt source, dynamically removed sulfur from the magmatic volatile phase (mvp) over the course of the run via the equilibrium

$$Pt^{\circ} + 1/2S_2^{mvp} = PtS. \quad (4)$$

EPMA-analysis of the Pt chips recovered from runs of different durations indicates that a sulfidation front propagated toward the center of the Pt chip. The sulfidation front was observed as a rind of PtS which thickens progressively with increasing run time. The subtly changing experimental fS_2 conditions are reflected compositionally in the dissolved sulfur content of the quenched silicate melt and also the metal content of the recovered mss. In light of the relatively small range in fS_2 values for a given assemblage, with respect to the long experimental run durations (a maximum difference of ~1.0 log unit for run durations in excess of 600 h is observed), we postulate that the composition of the experimental run products represents a steady state (on the time scale of 2–3 days) or perhaps an equilibrium state, reflective of the "instantaneous" fS_2 of the system. Thus, the quenched-in compositions of the experimental run products represent a snapshot of a system continuously evolving toward its final equilibrium fS_2 condition defined by the Pt–PtS buffer. The sluggish decline in fS_2 values (approximately 0.04 log units day^{-1}) coupled with the relatively high reactivity of the sulfide and silicate melt phases as observed in other studies at similar P–T conditions (e.g., Ballhaus and Ulmer, 1995; Clemente et al., 2004) suggests that the fS_2 of the system at the time of the termination of the run, is accurately reflected in the run products (i.e., the run products closely maintained an equilibrium relationship with system fS_2 as this parameter slowly changed). While the experiments did not reach a final "equilibrium" sulfidation state, the relative differences in the experimental partitioning behavior for Pt, Pd, Cu and Au place important constraints on the geochemical behavior of these metals in magmatic-hydrothermal systems.

2.4. Analytical procedures

2.4.1. EPMA analyses

Recovered glass (i.e., quenched melt) and sulfides were analyzed by using wavelength dispersive spectrometry (WDS) with a JEOL® JXA-8900 SuperProbe at the University of Nevada, Las Vegas. Glasses were analyzed for major elements using a 15 kV accelerating voltage and a 5 nA Faraday cage current. A 10 μm de-focused beam was used in conjunction with the low beam current in order to minimize current–flux–density-induced alkali diffusion (cf., Morgan and London, 1996).

The concentration of *S* in the quenched glasses was quantified by using a 10 μm diameter beam and a 50 nA Faraday cage current with counting times of 90 s on peak and 90 s on the background. The position of the *S* Kα peak was determined with a PET spectrometer for individual aliquots of experimental glass by using a statistical, automated peak search function in the JEOL® software. Natural ZnS was used as a standard for the *S* analysis. The applied ZAF matrix correction procedure for the S analyses employed the averaged major element composition of the glass as determined by the previously described analytical conditions. Calculated analysis-specific 3σ limits of detection (LOD) for *S* in the glasses range from 60 to 70 μg/g for the entire suite of analyses. The low concentration of *S* in the experimental glasses prevented us from using the peak shift in the *S* Kα radiation, determined by EPMA, to estimate the proportion of sulfide to sulfate species dissolved in the glass. However, considering the relatively low oxidation state of the runs (~NNO), we estimate that greater than 95% of the sulfur present in the melt is dissolved as the reduced species S^{2-} (cf., Carroll and Rutherford, 1988). Secondary standards VG-A99 and VG-2 were analyzed to evaluate the performance of the *S* analytical routine. Using our analytical routine, the concentration of *S* in standard glasses VG-2 and VG-A99 were quantified at 1300 ± 44 and 155 ± 9 μg/g, respectively. Previous studies that used EPMA to quantify the *S* content of VG-2 report 1403 ± 44 μg/g (O'Neill and Mavrogenes, 2002) and 1340 ± 80 μg/g (Dixon et al., 1991). The concentration of *S* in VG-2 has been reported as 1320 ± 50 μg/g when quantified by wet chemical methods (Wallace and Carmichael, 1992). The *S* content of VG-A99 as determined by EPMA has been reported as 138 ± 13 μg/g (Witter et al., 2005) and 170 ± 80 μg/g (Dixon et al., 1991). The agreement between our EPMA-determined S values and extant literature values suggests that the S concentrations reported herein are accurate.

Recovered Cu–Fe sulfide crystals were analyzed by using a 30 kV accelerating voltage and a 30 nA beam current. Iron, S, Ni and Cu were quantified by using Kα X-ray emission lines, whereas Pt, Pd and Au were quantified by using Lα X-ray emission lines in order to mitigate spectral interferences observed in the M series lines for these latter elements. A beam diameter of 15 μm was used in order to reintegrate the composition (presumably at run conditions) of the fine scale (<1 μm) exsolution features of the recovered sulfide material. Quenched sulfide melts were analyzed with a broad 40 μm beam to obtain the average composition of the sulfide melt at run conditions.

2.4.2. LA-ICP-MS analyses

LA-ICP-MS analyses were performed at the Institute for Isotopengeologie and Mineral Rohstoffe at ETH in Zürich, Switzerland by using a homogenized prototype Excimer ArF laser ($\lambda = 193$ nm) system, similar to the Geolas System, coupled with a Perkin-Elmer Elan 6100 DRC quadrupole ICP mass spectrometer. To improve the limits of detection for Pt, Pd and Au, a carrier gas mixture comprised of a helium (1.15 L/min) and hydrogen (6 ml/min) mixture was utilized (Guillong and Heinrich, 2007). The diameter of the ablation crater was varied from 90 μm for quenched glasses and mt to 30 μm for sulfide run products; ablations were carried out at an energy density of 25 J cm^{-1} and a repetition rate of 10 Hz for silicate glasses and mt. To improve the transient signal from the sulfides, the energy density was decreased to 10 J cm^2 and 3 Hz repetition rate. NBS-610 was utilized as a standard reference material for all investigated phases. Additionally, a synthetic PGE-doped Cu–Fe sulfide standard (Wohlgemuth-Ueberwasser et al., 2007) was utilized for Pt and Pd in some sulfide phases. The polyatomic interference from $^{65}Cu^{40}Ar^{+}$ produced in the plasma on the isotope ^{105}Pd is problematic for the analysis of Pd in Cu rich phases (i.e., iss). The $^{65}Cu^{40}Ar^{+}$ species production rate was quantified by ablating 99.999% Cu and measuring the resultant count rates on mass 65 and 105; $CuAr^{+}$ interference was measured to be 0.05% of the counts measured on mass 65. Based on this, the raw counts from ^{105}Pd can be corrected for interfering $^{65}Cu^{40}Ar^{+}$ species if necessary. The data indicate that the use of NBS-610 and the synthetic PGE sulfide standards to reduce and calculate Pd and Pt concentrations in sulfide phases yield statistically similar, albeit slightly different results. As discussed below, both the EPMA- and LA-ICP-MS-determined concentrations of Pd and Pt are presented to allow a comparison of the use of the silicate glass standard (i.e., NBS-610) vs. the synthetic PGE-doped standard to quantify Pd, Pt and Au concentrations. Data processing and reduction of the raw LA-ICP-MS data were performed by using SILLS (Guillong et al., 2008) using EPMA-determined element concentrations as the internal standard. Aluminum was used as the internal standard for the silicate glass analyses. Iron was utilized as the internal standard for mt, mss and iss.

3. RESULTS

3.1. Silicate glass from assemblages 1, 2 and 3

3.1.1. Major element and chlorine concentrations in the silicate glass

The silicate glass recovered from all runs is crystal free and homogenous within a given experiment with respect to the concentrations of Si, K, Na, Al and Cl (Table 3). The concentration of Fe exhibits slight variability; however, the range of Fe concentrations in silicate glass is consistent with that reported in previous experimental studies at similar conditions (e.g., Simon et al., 2008). The concentration of *S* in some recovered glasses exhibits slight heterogeneity; these values are attributed to uncertainty associated with analyzing low sulfur concentrations that are near the

Table 3
Elemental composition of run-product experimental glasses. Major element concentrations were quantified by using EPMA. The concentrations of Pt, Pd, Au and Cu were quantified by using LA-ICP-MS. ASI totals represent the molar ratio of Al_2O_3divided by the product of Na_2O and K_2O. Uncertainties are 1σ.

Run	Duration	SiO_2	FeO	K_2O	Na_2O	Al_2O_3	Cl	S (μg/g)	Cu (μg/g)	Pt (μg/g)	Pd (μg/g)	Au (μg/g)	Total	ASI
Iss + po + magnetite + rhyolite melt + aqueous supercritical fluid + Pt + Pd + Au; no HCl added to starting solution														
12	69	71.11 (0.75)	0.67 (0.10)	5.26 (0.21)	3.04 (0.19)	11.71 (0.21)	0.2 (0.02)	152 (39)	8 (2)	1.2 (0.17)	0.34 (.31)	0.65 (0.49)	91.64	1.09
13	167	70.87 (0.49)	0.55 (0.05)	4.96 (0.17)	2.99 (0.10)	11.69 (0.17)	0.15 (0.15)	233 (48)	6 (1.4)	0.893 (0.03)	0.16 (.09)	0.038 (0.01)	91.53	1.14
15	360	71.89 (0.75)	0.73 (0.03)	5.32 (0.21)	3.13 (0.06)	11.65 (0.28)	0.2 (0.01)	245 (44)	13.6 (4)	0.266 (0.37)	0.21 (.22)	0.086 (0.04)	92.72	1.07
Iss + po + magnetite + rhyolite melt + aqueous supercritical fluid + Pt + Pd + Au; NaI/KI/H of starting solution equals one														
46	160	70.45 (0.52)	0.90 (0.43)	5.90 (0.10)	3.17 (0.09)	11.54 (0.22)	0.18 (0.04)	152 (49)	4.8 (0.89)	1.03 (0.15)	0.074 (0.05)	0.043 (0.02)	91.97	0.99
47	336	71.55 (0.60)	0.94 (0.05)	5.83 (0.11)	2.99 (0.09)	11.29 (0.18)	0.18 (0.02)	227 (49)	9.6 (2)	0.046 (0.03)	NA	0.35 (0.30)	91.88	1.01
48	483	70.78 (0.41)	0.96 (0.05)	5.9 (0.10)	3.06 (0.08)	11.67 (0.21)	0.21 (0.03)	184 (34)	6.7 (1)	0.17 (0.11)	0.046 (0.046)	0.100 (0.02)	91.98	1.02
49	607	72.68 (0.30)	0.59 (0.07)	5.42 (0.17)	2.85 (0.09)	11.10 (0.21)	0.13 (0.01)	153 (14)	4.8 (1.9)	0.01 (0.01)	0.033 (0.027)	0.06 (0.03)	92.69	1.05
50	672	72.34 (0.26)	0.71 (0.04)	5.63 (0.11)	2.92 (0.08)	11.28 (0.27)	0.15 (0.01)	143 (9)	5.2 (1.4)	0.027 (0.02)	0.010 (0.01)	0.019 (0.01)	92.83	1.05
Iss + bn + magnetite + rhyolite melt + aqueous supercritical fluid + Pt + Pd + Au														
32	140	71.08 (0.4)	0.52 (0.2)	5.89 (0.2)	2.93 (0.34)	11.51 (0.18)	0.14 (0.03)	151 (19)	13 (1.4)	1.1 (0.11)	0.02 (0.01)	0.14 (0.11)	91.77	1.03
33	231	72.46 (0.7)	0.34 (0.04)	5.68 (0.14)	2.57 (0.32)	11.26 (0.20)	0.09 (0.02)	83 (27)	NA	NA	NA	NA	91.52	1.09
34	281	71.09 (0.5)	1.91 (0.2)	5.49 (0.3)	2.99 (0.15)	10.55 (0.6)	0.18 (0.10)	74 (17)	22 (21)	0.6 (0.04)	0.027 (0.01)	0.18 (0.13)	91.62	0.97

NA, not analyzed.

detection limit. EPMA data indicate that all glasses are slightly peralkaline to peraluminous; the aluminum saturation index (ASI), the ratio of Al/Na + K, ranges from 0.97 to 1.14. The solubility of water in the melt, estimated by using the EPMA difference method, ranges from 7 to 8.5 wt.%. This estimate is consistent with the expected water solubility of 6–8 wt.% in rhyolite melt at 800 °C and 150 MPa (McMillan and Holloway, 1987).

3.1.2. Cu, Au, Pt and Pd concentrations in the silicate glass

The major and trace element concentrations including Cu, Au, Pt and Pd in the recovered silicate glasses are provided in Table 3. The concentration of Cu in silicate glass ranges from 5 to 22 μg/g and is homogeneously distributed within glass beads recovered from all runs. These values are consistent with the published Cu concentrations of 4 μg/g (Lynton et al., 1993), 26 μg/g (Jugo et al., 1999) and 1 μg/g (Simon et al., 2006) for similar bulk assemblages at similar experimental conditions. In this study, melts reacted with low sulfidation Cu-rich phase assemblages have the highest Cu concentrations, whereas high sulfidation Cu-poor phase assemblages generally yield lower Cu concentrations in rhyolite melt.

The quantification of the concentrations of Au, Pt and Pd in recovered silicate glass is complicated owing to the observed heterogeneous distribution of these metals in glass (Fig. 1a and b). Several previous studies have discussed the inherent difficulty in quantifying the solubility of noble metals in quenched silicate melts with oxidation states lower than the mt–hematite buffer. The LA-ICP-MS spectra from ablation of silicate glasses are routinely complicated by the presence of spatially heterogeneous distributions of some metals (e.g., Ag; Simon et al., 2008). This so called "nano-nugget effect" (cf., Borisov and Palme, 1997; Ertel et al., 1999; Simon et al., 2007), as observed in LA-ICP-MS spectra has been interpreted previously as either a quench-exsolution phenomenon (e.g., Cottrell and Walker, 2006) or as a product of redox reactions within the charge (e.g., Ertel et al., 1999). Stable PtO species within the melt structure are reduced to elemental Pt in colloidal suspension within the melt (Ertel et al., 1999) as a function of the reduction of the experiment oxidation state during run up. Simon et al. (2008) suggest that initial noble metal solubilities in the melt are relatively high, approaching the 10 μg/g range, over the first 12–24 h of a run before the experimental charge comes to equilibrium with the intrinsic redox state of the pressure vessel; hence, an excess of Pt is initially dissolved in the melt. As the charge approaches osmotic redox equilibrium, the fO_2 of the metal-oversaturated melt decreases. During the period of reduction the melt gradually exsolves excess Pt, Pd and Au, forming nano-nuggets, until the melt fO_2 reaches the buffered value of ~NNO. Ertel et al. (1999) demonstrated that during a period of fO_2 reduction, Pt and Rh solubilities decrease in the melt, causing the melt to exsolve the excess metals and forming nano-nuggets until the melt fO_2 reaches its final state. We specifically note the congruency of the Pd, Au and to a much lesser extent Cu in LA-ICP-MS signals from the nugget bearing analyses (Fig. 1a). Such signals have the appearance that the nugget-forming metals are either

alloyed or enjoy an intimate, mechanical association. Only nugget free analyses of silicate glasses (Fig. 1b) have been considered in this study, as these LA-ICP-MS signals are assumed to approximate best the equilibrium solubility of the noble metals in the melt.

The measured solubility of Au in silicate glass from individual runs and among runs in the present study is variable (see Table 3). The data in the present study indicate that the best estimate for Au solubility in S-bearing rhyolite melt is on the order of a few tens to a few hundreds of ng/g (Table 3). Frank et al. (2002) reported that Au solubility at 800 °C and 100 MPa in a S-free Au-saturated rhyolite melt is 1 μg/g. As discussed by Frank et al. (2002), it is possible that the quenched silicate glasses produced in their experiments contained submicroscopic gold particles or regions of increased Au concentration within the glass that formed during quenching. Frank et al. (2002) discussed the nugget effect, with specific reference to Instrumental Neutron Activation Analysis (INAA) and Secondary Ion Mass Spectrometry (SIMS), and concluded that the best estimate of Au solubility in S-free rhyolite melt was on the order of 1 μg/g. Simon et al. (2005) used nugget-free LA-ICP-MS analyses to quantify that the solubility of Au in S-free rhyolite is on the order of 500 ng/g. Jugo et al. (1999) reported Au solubility in S-bearing Au-saturated rhyolite melt, saturated with iss and po at 850 °C and 100 MPa, to be on the order of 2–4 μg/g. Simon et al. (2007) report that the solubility of Au in S-bearing rhyolite, equilibrated with arsenopyrite (FeAsS), is 0.6 μg/g. All of these experimental studies were conducted at broadly similar fS_2, fO_2, pressure and temperature conditions. We suggest that the higher reported Au solubility values may reflect the nature of the analytical technique. Jugo et al. (1999) and Frank et al. (2002) used the bulk analytical technique INAA which would incorporate Au nuggets and include them in the analytical totals. The solubilities of Au in assemblages 1, 2 and 3 are 0.26 ± 0.34, 0.11 ± 0.13 and 0.16 ± 0.03 μg/g, respectively; the average solubility is 0.18 ± 0.07 μg/g. As stated above, the uncertainties do not reflect the presence of nuggets in the integrated portion of the signal. In light of the aforementioned issues, we suggest that the data in the current study constrain the solubility of Au in S-bearing rhyolite melt, at the PTX conditions in this study, to no more than a few 100 ng/g, consistent with previous studies.

The concentrations of Pt and Pd in silicate glass are reported in Table 3. A systematic decrease in the abundances of Pt and Pd in the quenched melt occurs as a function of increasing run duration for each experimental assemblage (Fig. 2). Decreasing metal concentrations may be a function of the temporal evolution of the redox state of the system (initially) and/or by the additional possibility of decreasing the activities of the soluble metals or metal alloys in the experimental system via sulfidation and progressive alloying of elemental metallic species (i.e., the Pt and Pd metal chips used as the source of Pt and Pd). Platinum dissolution into the silicate melt structure may occur via the reaction proposed by Borisov and Palme (1997)

$$Pt^{metallic} + 1/2O_2^{system} = PtO^{melt} \quad (5)$$

with the corresponding equilibrium constant written as:

$$K_3 = \frac{xPt^{metallic}\gamma Pt^{metallic}}{xPtO^{melt}\gamma PtO^{melt}} \cdot fO_2^{-1/2} \quad (6)$$

where x and γ are the mol fraction and activity coefficient, respectively. The numerator of the expression may be written as:

$$xPt \cdot \gamma Pt = aPt \quad (7)$$

where a is the activity of Pt in Eq. (5). The solubility of Pt, as expressed in Eq. (4), is a function of the activity of Pt in the source phase, a_{Pt}^{source}, (i.e., native metal, metallic alloy, or sulfide) and the fO_2 imposed on the system. The choice of PtO as the stable Pt species in the melt is based on the strong positive correlation observed between Pt solubility and fO_2 reported by Ertel et al. (1999). Eq. (4) governs the solubility of Pt as a divalent oxide species within the silicate melt structure.

The observed decrease in the measured abundances of Pt and Pd in the quenched glasses (Fig. 2) with increasing run duration may reflect the decreasing activity of Pt and Pd in the experimental system as governed by the interaction of sulfur in the aqueous phase with alloys of the Pt and Pd foils via the following sulfidation reaction:

$$xPt^{source} + (1-x)Pd^{source} + 1/2S_2^{vapor} = (Pt_xPd_{1-x})S \quad (8)$$

The activity of Pt in the system may be further decreased via the addition of Pd and Fe in solid solution on the PtS lattice. A similar relationship was also noted by Li et al. (2003) for Ni in S bearing magmas. The a_{Pt}^{source} is defined by the equilibrium expression in Eq. (6) where:

$$a_{Pt}^{source} = \left(\frac{a_{(Pt,Pd)S}}{(a_{Pd}^{metal})^{1-x} \cdot (fS_2^{vapor})^{1/2} \cdot K_5} \right)^{1/x} \quad (9)$$

Substitution of the expression for Pt activity derived in Eq. (7) into the numerator of the equation governing Pt solubility as an oxide species (Eq. (4)) clearly shows that Pt solubility in the silicate melt phase in the investigated system is not only proportional to the oxygen fugacity of the system, but a complex function of the fS_2 imposed on the experimental system and the composition of the phase acting as the Pt source to the melt. The a_{Pt}^{source}, as defined in Eq. (7), via progressive reaction of elemental Pt with Pd, S and Fe, will decrease until the composition of the Pt–Pd–Fe–S overgrowths on the Pt metal come to equilibrium with the system. Only then will the a_{Pt}^{sys} be fixed. Thus, it is predicted that Pt solubility in the melt in sulfide–oxide–silicate melt systems should vary with changes in the fO_2, fS_2 and the a_{Pt}^{source} of the experimental system. Platinum solubility in the experimental system is thusly controlled by the variables fS_2 and fO_2 where a_{Pt}^{metal} of the source is a function of the fS_2 imposed on the experimental system.

3.1.3. Mss composition

Recovered mss varies remarkably little in the S to Σ Fe–Pd–Pt–Au–Cu ratio within a set of analyses for multiple grains from individual experiments. Mss from nearly all runs contains measurable quantities of Ni, an element which is not present at measurable concentrations in any of the starting materials. Nickel may be introduced via the diffusion of Ni through the Au capsule from the pressure vessel via the water

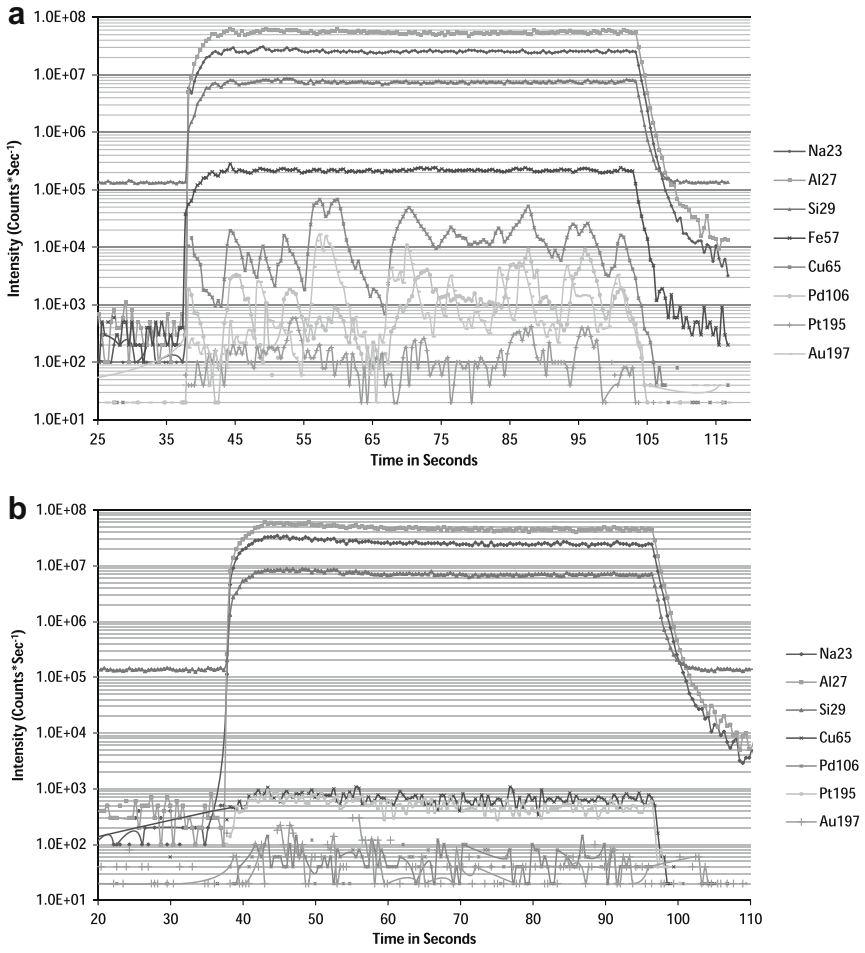

Fig. 1. (a) Nano-nugget bearing LA-ICP-MS signal from quenched silicate melt. Note the congruency of Cu, Au and Pd signals; additionally note the homogenous Fe signal. The homogenous nature of the Fe signal suggests that the nano-nuggets observed in the signal are not an artifact induced by small scale crystalline sulfide inclusions, but are in fact nano-nuggets analogous to those observed in other experimental studies. (b) Nano-nugget "free" LA-ICP-MS signal from quenched silicate melt. All metal signals display some small degree of heterogeneity, however, these signals are comparatively homogenous with respect to the signal in Fig. 1a.

pressure medium and direct mechanical contact of po with the Au metal capsule as observed in previous experimental studies (Scaillet and MacDonald, 2001). The composition of mss is provided in Table 4. The solubility of Au in mss in the current study is of 170 ± 71 μg/g, similar to the value of 470 μg/g for Au solubility in mss reported by Jugo et al. (1999) at similar pressure–temperature-composition (PTX) conditions; log fS_2 values overlap statistically in both studies.

Ubiquitous exsolution features (Fig. 3) less than 1 μm in width were observed in most of the recovered mss crystals. Although the exsolution features were too small to be individually resolved quantitatively with EMPA-WDS or LA-ICP-MS, the exsolution features have been qualitatively characterized chemically by using energy dispersive X-ray spectrometry (EDS) and identified as predominately Pd–Cu–Ni-rich-sulfide relative to the host mss. Exsolution features observed in mss are likely the product of a relatively slow quench rate; i.e., ~2 min. The solubilities of Pt and Pd in mss have been demonstrated to be a strong function of temperature (Ballhaus and Ulmer, 1995). The presence of quench-exsolution texture in our experimental mss is consistent with the down-temperature decrease in Pt and Pd solubility observed by Ballhaus and Ulmer (1995). Mss at run conditions is expected to take on the hexagonal structure with a fully disordered Fe sublattice; however, upon termination of the run, ordering of the vacancies on the Fe sublattice and eventual conversion or partial conversion to a monoclinic form, is speculatively responsible for the pervasive exsolution textures.

Integration of the composition of the exsolution features with the composition of the matrix mss is required to accurately quantify the concentration of these elements at run conditions. We used a 30 μm beam diameter for both EPMA and LA-ICP-MS analyses of mss. The data reported in Table 4 indicate that both methods effectively reintegrate the mss and exsolution lamellae and yield similar metal concentrations. The reported EPMA-determined concentrations of Fe and Cu suggest that both metals are homogenously distributed in the mss.

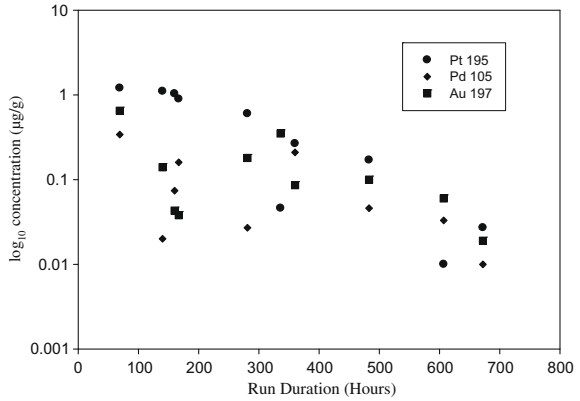

Fig. 2. The concentration of Pt, Pd and Au in the silicate melt as a function of run duration. The uncertainties on each datum are smaller than the symbol size.

3.1.4. Iss composition

Intermediate solid solution was observed in all run products; however, the iss observed in runs 32, 33 and 34 is inter-grown with bn and is thought to have exsolved from the sulfide melt, discussed below, during quench. Iss from these three runs is thus not reported as it was reintegrated into the sulfide melt composition. The measured compositions of iss reported in Table 5, is similar in all experiments. The composition of run product iss deviates significantly from the stoichiometry of the starting chalcopyrite. Total *S* content of recovered iss appears to vary little from the average value of ~35.0 wt.%. Platinum and Pd concentrations in iss were generally near or below the EPMA limit of detection, whereas Au concentrations within individual iss crystals in a given experiment exhibited variability. We hypothesize that the observed heterogeneity of Au within recovered iss is a quench phenomenon; i.e., the presence of Au lamellae in iss, observed by using back scattered electron (BSE) imaging, indicate exsolution of Au during quench as reported by Jugo et al. (1999). The concentration of Au in run-product iss in the current study ranges from 0.37 to 0.72 wt.%, with an average on the order of 0.5 wt.%. This is similar, albeit lower than the experimentally determined value ($\pm 1\sigma$) of 1.9 ± 0.4 wt.% for Au solubility in mss reported by Jugo et al. (1999).

3.1.5. Sulfide melt

The run products from charges loaded initially with cp and bn contain a single sulfide entity that we interpret to be a quenched sulfide liquid (Fig. 4). The sulfide entity encapsulates entire mt crystals and the boundary between the two appears to be a wetting surface. The EPMA-determined composition of the sulfide melt phase is provided in Table 6. This phase exhibits a complex intergrowth texture between Cu-rich and Fe-rich sulfide phases. The average composition provided in Table 6 reflects the inherent difficulty in reintegrating such a complex quench phase. Sulfide quench textures in our runs are consistent with the observed sulfide quench textures from other studies of sulfide melts (cf., Ripley et al., 2002). Recently revised phase relations for the Cu–Fe–S–O system from Tsujimura and

Table 4
Composition of recovered monosulfide solid solution. Fe, S, Cu and Ni quantified by EPMA. Pd, Pt and Au were quantified by using both EPMA and LA-ICP-MS. The LA-ICP-MS spectra for Pd and Pt were reduced using both a synthetic Pt-, Pd-bearing sulfide standard and also NBS-610; denoted as EPMA and NBS-610, respectively. Uncertainties are 1σ.

Run #	Fe wt.%	S wt.%	Cu wt.%	Ni wt.%	Pd (EPMA) wt.%	Pd (sulfide) (µg/g)	Pd (NBS-610) (µg/g)	Pt (EPMA) (µg/g)	Pt (sulfide) (µg/g)	Pt (NBS-610) (µg/g)	Au (NBS-610) (µg/g)	Au (EPMA) (µg/g)	Total
12	55.08 (0.87)	40.18 (0.38)	2.16 (0.71)	0.05 (0.007)	2.38 (0.50)	2.87 (0.15)	3.3 (0.18)	<DL	24 (1.3)	13 (.79)	131 (79)	<DL	100.69 (0.3)
13	53.17 (0.23)	38.9 (0.51)	4.83 (0.77)	0.05 (0.004)	2.44 (1.73)	NA	NA	<DL	NA	NA	NA	<DL	99.54 (0.7)
15	49.71 (1.6)	39.69 (0.36)	2.77 (NA)	5.3 (0.36)	2.33 (0.69)	2.31 (0.06)	2.54 (0.1)	0.33(0.18)	470 (40)	1789 (170)	230	<DL	100.07 (0.7)
46	55.08 (1.2)	38.9 (0.22)	4.14 (1.09)	0.14 (0.05)	0.90 (0.42)	NA	0.5 (0.13)	<DL	NA	108 (52)	108	<DL	100.28 (0.5)
47	53.5 (1.1)	38.91 (0.55)	5.01 (2.62)	0.43 (0.17)	1.31 (0.26)	NA	1.2 (0.1)	0.06	NA	236 (40)	136	<DL	100.35 (0.3)
48	53.42 (1.9)	38.63 (0.7)	5.41 (2.67)	0.51 (0.07)	1.18 (0.56)	NA	1.41 (0.02)	0.18 (0.04)	NA	561 (24)	286 (68)	<DL	100.31 (0.5)
50	53.31 (1.4)	38.98 (0.48)	5.10 (2.06)	0.32 (0.02)	1.79 (0.25)	NA	1.9 (0.08)	0.22 (0.02)	NA	910 (195)	134 (24)	<DL	100.53 (0.5)
34	58.78 (0.46)	37.32 (0.23)	4.10 (0.61)	<DL	<DL	NA	NA	<DL	NA	NA	9.1 (5.3)	<DL	100.37 (0.2)

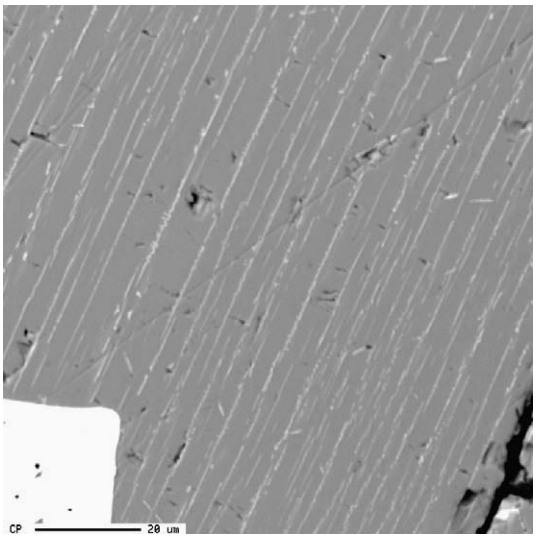

Fig. 3. BSE image of fine scale exsolution textures in mss; exsolution features are a Pd–Ni–Cu rich sulfide. The high Z# phase in the lower left hand corner is metallic Au. The scale bar is 20 μm.

Kitakaze (2004) place the melting temperature for the dry iss-bornite system at less than 800 °C, the temperature of experiments in the current study. Experiments in this study were performed at water-saturated conditions and the effect of fH_2O on sulfide melt–solid phase relations is unknown. We did not attempt to quantify the oxygen content of the sulfide melt phases owing to the relatively slow quench rate which likely promoted the extensive crystallization of the sulfide melt phase which renders it unlikely that the original oxygen content of the sulfide liquid was preserved.

3.1.6. Magnetite

Magnetite was recovered in all successful experimental runs. The concentrations of all analyzed metals (Au, Cu, Pd and Pt) in mt are on the order of a few ng/g. EPMA analyses of run-product mt indicate that the final composition is near stiochiometric end-member mt.

3.2. Evaluation of experimental sulfur fugacity

Sulfur fugacity was calculated by using the measured *S* solubilities of the recovered experimental glasses following Toulmin and Barton (1964) and the empirical model of Clemente et al. (2004). In the Clemente et al. (2004) model, fS_2 values are calculated relative to the metallic Fe-troilite sulfidation (FFS) buffer, utilizing an internally consistent fO_2 corresponding to NNO + 0 for all of the experimental runs. Eq. (6) was used to calculate fS_2 values

$$\Delta FFS = \frac{\log S(ppm) - 0.001T + 0.2567(\Delta NNO)}{0.1713 + 0.0034(\Delta NNO)}. \quad (10)$$

where Δ FFS is the log fS_2 value defined relative to the FFS buffer. Sulfur fugacity was also calculated by using the $Fe_{(1-x)}S$ indicator method, formulated by Toulmin and Barton (1964) as

Table 5
Composition of recovered intermediate solid solution Fe, S, Cu and Ni quantified by EPMA. Pd, Pt and Au were quantified by using both EPMA and LA-ICP-MS. The LA-ICP-MS spectra for Pd and Pt were reduced using both a synthetic Pt-, Pd-bearing sulfide standard and also NBS-610; denoted as EPMA and LA-ICP-MS, respectively. Uncertainties are 1σ.

Run #	Fe wt.%	S wt.%	Cu wt.%	Ni wt.%	Pd (EPMA) wt.%	Pd (sulfide) (μg/g)	Pd (NBS-610) (μg/g)	Pt (EPMA) (μg/g)	Pt (sulfide) (μg/g)	Pt (NBS-610) (μg/g)	Au (NBS-610) (μg/g)	Au (EPMA) (μg/g)	Total
12	37.23 (0.91)	35.28 (0.28)	27.24 (1.01)	<DL	<DL	NA	311 (387)	<DL	NA	0.62 (0.5)	5585 (14)	2100 (2500)	100.17 (0.4)
13	38.54 (0.19)	34.98 (0.25)	26.43 (0.04)	<DL	<DL	NA	64 (76)	<DL	NA	7.1 (1.9)	7220 (1256)	3080 (490)	100.29 (0.4)
15	38.03 (0.11)	34.74 (0.15)	27.64 (0.07)	<DL	<DL	NA	1541 (94)	<DL	NA	862 (16)	107 (55)	<DL	100.51 (0.1)
46	35.48 (1.3)	35.13 (0.38)	28.19 (0.71)	<DL	<DL	NA	93 (46)	<DL	NA	4.3 (0.8)	3706 (1483)	<DL	99.14 (0.7)
47	37.85 (0.15)	34.82 (0.35)	26.96 (0.40)	<DL	<DL	NA	114 (49)	<DL	NA	19 (29)	4404 (1153)	<DL	99.76 (0.1)
48	38.75 (0.15)	34.83 (0.13)	25.82 (0.17)	0.12 (0.01)	<DL	NA	NA	<DL	NA	NA	NA	NA	99.73 (0.2)
49	37.39 (0.35)	35.45 (0.15)	26.78 (0.38)	0.08 (0.01)	<DL	NA	172 (196)	<DL	NA	1.99 (0.4)	6771 (1895)	1400 (1400)	100.24 (0.2)
50	37.62 (0.44)	35.2 (0.22)	26.97 (0.33)	<DL	<DL	NA	276 (183)	<DL	NA	62 (117)	5693 (1739)	1100 (2400)	100.02 (0.4)

$$\log_{10} fS_2 = (70.03 - 85.83x)(1000/T - 1) + 39.30 \times \sqrt{1 - .9989x} - 11.91 \quad (11)$$

where x represents the mole fraction of the FeS component of mss. Palladium, Pt, Au, Cu and Ni have been assumed to substitute ideally for Fe in the mss lattice on a one to one basis (cf., Jugo et al., 1999). The effect of these metals on the mss solution behavior is assumed to be ideal given the low measured concentrations of these metals in mss. Values for fS_2 calculated by both methods are reported in Table 7. The fS_2 values from experimental runs have been plotted relative to the liquid sulfur condensation curve, Pt–PtS buffer, and the metallic FFS buffer curve in Fig. 5. We suggest that the observed discrepancies between fS_2 values calculated from the two methods may reflect the kinetically sluggish nature of *S* dissolution into the melt (i.e., minor disequilibrium with respect to *S* solubility in the melt phase). Additionally, in runs 33 and 34, some individual EPMA analyses of *S* in the glass were at or below the detection limit. The average sulfur concentration for these runs included only values that were above the EPMA limit of detection; thus, it is likely that fS_2 values calculated from the EPMA averages for these runs are systematically biased toward higher values. We suggest that using the mss composition to calculate the fS_2 of a system is a more robust method than using the sulfur content of the silicate melt owing to the much higher degree of complexity in the solution behavior of the latter. Additionally the mss composition appears to be temporally more responsive to changing fS_2 conditions.

Sulfur fugacity values calculated from both methods appear to converge in experimental runs of intermediate duration. This reflects the attainment of a steady state with respect to both S solubility in the silicate melt and the metal composition of the recovered mss. We interpret this decrease in calculated fS_2 values to be a function of the progressive sulfidation of the Pt and Pd metal loaded initially as a metal source for the experiments. The reaction of the finite reservoir of sulfur within the experimental charge with the metal sources (i.e., the Pt and Pd foil chips) should result in depletion of the sulfur within the supercritical aqueous fluid phase with increasing progress of favorable Pt and Pd sulfidation reactions. Evidence for the progressive removal of *S* from the supercritical aqueous fluid phase was observed in the form of the development of a PtS "rind" on the recovered pieces of Pt metal foil. Evidence for the removal of *S* from the supercritical aqueous fluid phase is also observed in the systematic decrease of the calculated fS_2 values for the runs. Analogous Cu–sulfide overgrowths have been observed encapsulating molten Cu metal blebs in a study of Cu solubility in mafic silicate melts (Holzheid and Lodders, 2001). The advancing sulfidation front (Figs. 6 and 7) is truncated at the interface with elemental Pt. This elemental Pt forms the core of the recovered foil chip. No elemental Pd was recovered in any of the runs indicating that all Pd present was either lattice bound in mss and Cu–Fe sulfide phases, alloyed with Au and Pt, or bound in separate, ubiquitous PdS phases.

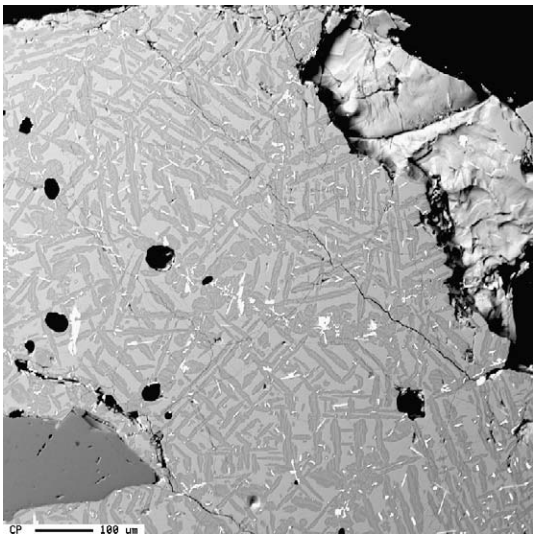

Fig. 4. BSE image of a sulfide entity interpreted to be a recrystallized sulfide liquid. Dark and light grey intergrowths are iss and bn. The scale bar is 100 μm. The dark grey crystal at lower left is magnetite which coexisted with the sulfide liquid at run conditions.

4. DISCUSSION

4.1. Fractionation of Pt, Pd and Au in nature: the effect of fO_2 and fS_2

The new data place constraints on the relative fractionation effects induced by the precipitation of mss, iss and sulfide–oxide melts on the abundances of Pt, Pd and Au in silicate magma. Silicate melts can reach sulfide saturation owing to magmatic fractionation or the addition of *S* sourced from outside of the magma (e.g., assimilation of biogenic pyrite from a sedimentary sequence). Both processes result in an increase in the aS_2 in the melt, hence promoting the saturation of the silicate melt with a sulfide phase. It is the fO_2–fS_2 condition at which sulfide saturation occurs that ultimately controls which sulfide phase will be stable (cf., Jugo et al., 1999), and how it will affect the Pd–Pt–Au budget of the evolving magmatic system prior to the exsolution of an aqueous magmatic volatile phase. Here we discuss the effects of mss, iss and sulfide melt on modifying the metal budget of magmatic systems.

4.1.1. The effect of mss saturation

The data in this study suggest that saturation of a magmatic system with mss should strongly fractionate Pd from Pt, and both of these PGE from Au. In addition to fractionation effects, the ability for mss to scavenge Pt and Pd from a silicate melt is dependent upon the fS_2 of the system; i.e., higher fS_2 yields higher Pt and Pd solubilities in mss. This relationship is consistent with the results of Ballhaus and Ulmer (1995); however, the absolute concentrations of both Pt and Pd in mss in this study are lower than the values reported by Ballhaus and Ulmer (1994) for experiments performed at identical temperatures similar fS_2 values. Discrepancies between the solubility data in the two studies

Table 6
Individual EPMA point analyses of quenched sulfide liquid for Run 32, 33 and 34. Note the heterogeneous distribution of Au. Each point analysis was performed using a broad, 40 μm beam in an attempt to reintegrate the composition of the sulfide liquid to that of run conditions.

	Fe	S	Ni	Pd	Pt	Au	Cu	Total
	Run 32 quenched sulfide							
	20.6	30.21	0.09	<DL	<DL	0.04	49.3	100.31
	18.4	29.05	0.08	0.04	<DL	1.5	51.38	100.5
	22.27	30.95	0.13	0.12	<DL	6.41	41.63	101.54
	18.62	29.28	0.05	<DL	<DL	0.07	53.02	101.06
	21.76	30.63	0.1	<DL	<DL	1.33	45.81	99.64
	20.97	30.24	0.06	<DL	<DL	0.15	48.63	100.09
	22.44	31.1	0.12	0.13	<DL	4.71	42.77	101.28
	19.87	29.7	0.15	0.02	<DL	0.92	48.52	99.2
	23.53	30.81	0.11	0.02	<DL	1.49	42.98	98.97
	18.92	28.64	0.07	0.05	<DL	2.44	50.53	100.67
Mean	**20.74**	**30.06**	**0.10**	**0.06**	**NA**	**1.91**	**47.46**	**100.33**
1 σ	**1.77**	**0.86**	**0.03**	**0.05**	**NA**	**2.11**	**3.95**	**0.86**
	Run 33 quenched sulfide liquid							
	26.96	30.8	<DL	<DL	<DL	<DL	41.81	99.6
	26.44	30.29	<DL	0.05	<DL	<DL	43.2	100.01
	26.61	30.25	<DL	<DL	<DL	0.02	43.13	100.05
	27.59	31.86	<DL	0.02	<DL	0.16	41.12	100.78
	26.44	30.85	<DL	<DL	<DL	0.03	42.83	100.19
	26.91	30.93	<DL	0.04	<DL	0.57	42.24	100.72
	26.43	29.83	<DL	0.05	<DL	0.09	44.41	100.85
	26.58	30.09	<DL	0.04	<DL	0.1	44.34	101.18
Mean	**26.75**	**30.61**	**NA**	**0.04**	**NA**	**0.16**	**42.89**	**100.42**
1 σ	**0.40**	**0.64**	**NA**	**0.01**	**NA**	**0.21**	**1.15**	**0.54**
	Run 34 quenched sulfide liquid							
	23.56	28.65	<DL	0.02	<DL	0.17	47.84	100.26
	33.03	30.73	<DL	0.3	<DL	0.41	35.13	99.62
	35.87	31.46	<DL	0.24	<DL	0.19	30.72	98.51
	19.44	27.41	<DL	<DL	<DL	0.07	52.02	98.96
	18.33	26.57	<DL	0.1	<DL	<DL	53.48	98.5
	17.95	26.66	<DL	<DL	<DL	0.14	54.3	99.05
	28.75	29.63	<DL	<DL	<DL	0.06	42.27	100.72
	32.33	30.41	<DL	0.38	<DL	0.05	37.95	101.13
	19.81	27.34	<DL	0.02	<DL	<DL	53.08	100.26
	22.64	28.22	<DL	<DL	<DL	0.17	49.67	100.73
	18.17	26.99	<DL	<DL	<DL	0.11	54.31	99.59
Mean	**24.53**	**28.55**	**NA**	**0.18**	**NA**	**0.15**	**46.43**	**99.76**
1 σ	**6.74**	**1.75**	**NA**	**0.15**	**NA**	**0.11**	**8.52**	**0.93**

may be attributed to the more complex nature of the solid solutions utilized in the current study. Ballhaus and Ulmer (1994) equilibrated mss with either Pt or Pd, but never both simultaneously; additionally, their study did not include additional competing metals. The current study has utilized assemblages containing a more complex metal assemblage, thus, we hypothesize that more complex assemblages may be the cause of the variability in measured solubility values. The presence of Cu at several wt.% and Ni at slightly less than 1 wt.% may inhibit the solubility of Pt and Pd on the Fe sublattice of the mss lattice. Future work is planned to quantify the crystallographic residency of metals in mss solid solutions.

To calculate Nernst-type partition coefficients for Pt, Pd and Au between rhyolite melt and mss, taking into consideration the variation in values determined in this study, we used lower and upper values for each metal as a limiting case. Using a lower and upper solubility value of 0.1 and 0.5 μg/g for Pt, Pd and Au in the rhyolite

Table 7
Sulfur fugacity of experimental run. Uncertainties are 1σ.

Run #	Duration (h)	S in glass (μg/g)	log fS_2[b] (bar)	log fS_2[c] (bar)
12	69	152 (39)	−1.05	0.07
13	167	233 (48)	0.02	−0.52
15	360	245 (24)	0.15	−0.14
46	160	152 (49)	−1.05	−0.92
47	336	227 (49)	−0.03	−0.87
48	483	185 (34)	−0.56	−0.86
49	607	153 (14)	−1.02	−0.90
50	672	143 (10)	−1.19	−0.76
32	140	151 (19)	−1.06	NR[a]
33	231	87 (20)	−3.21	NR[a]
34	281.5	73 (17)	−3.64	−5.16

[a] NR indicates that mss was not recovered from the charge.
[b] Sulfur fugacity calculated by using the Clemente et al. (2004) empirical algorithm.
[c] Sulfur fugacity calculated by using the Toulmin and Barton (1964) algorithm.

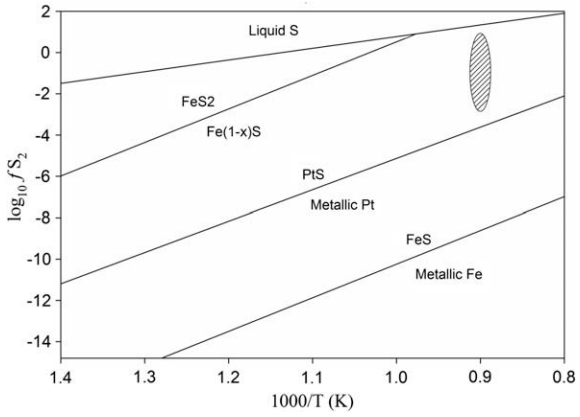

Fig. 5. Plot of fS_2 buffer curves relevant to calculated experimental sulfur fugacity values. Experimental fS_2 values are schematically represented by the stippled ellipse. Buffer curves modified after Fleet et al. (1999).

melt yields apparent Nernst-type partition coefficients that range from a low of $D_{Pd}^{mss/melt} = 4.4 \times 10^4$ to a high of $D_{Pd}^{mss/melt} = 2.2 \times 10^5$. Similarly for Pt, $D_{Pt}^{mss/melt}$ ranges from a low of 6×10^3 to a high of 3×10^4. These calculated $D^{mss/melt}$ values indicate that crystallization of mss leads to significant fractionation of Pt from Pd during silicate melt solidification. Thus, during mss fractionation, the absolute concentration of Pd in the silicate melt may decrease by a factor 10 relative to the concentration of Pt in the silicate melt. Gold is the most refractory of the three metals with measured concentrations in the silicate melt ranging from 0.35 to 0.01 μg/g with an average on the order of 0.1 μg/g. These Au solubility values yield a minimum $D_{Au}^{mss/melt} = 2.3 \times 10^3$ and a maximum $D_{Au}^{mss/melt} = 1 \times 10^4$. A comparison of these new results

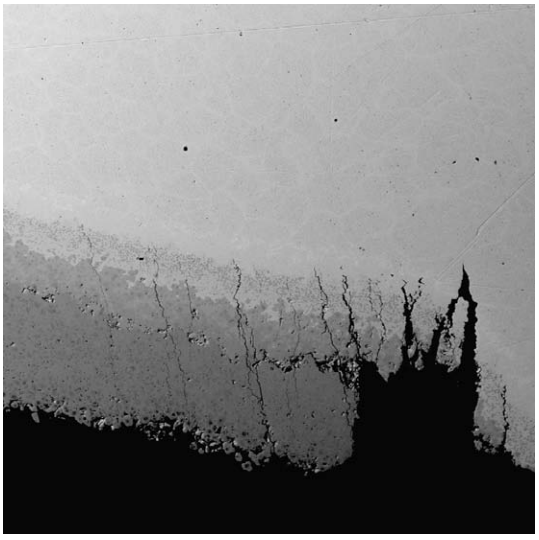

Fig. 6. An advancing sulfidation front in Pt foil chip in run of 360 h. Outer rim becomes (Pt, Pd, Fe) S in composition, where as the inner portion of the sulfidation front is nearly pure PtS grading into metallic Pt.

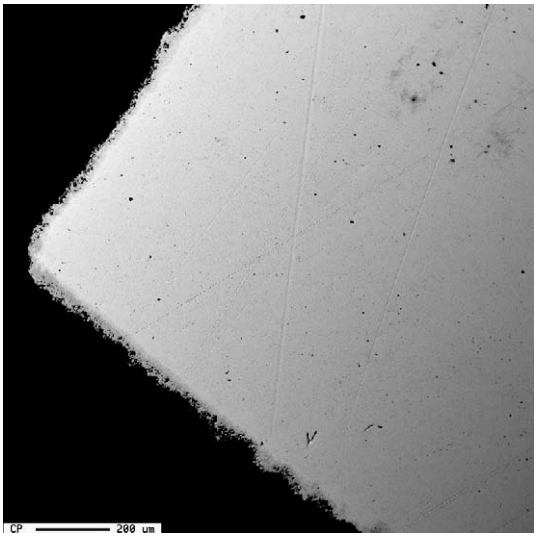

Fig. 7. Thin sulfidation rim (dark gray rimming the light grey) on a Pt foil chip in run of 67 h.

with those of Ballhaus and Ulmer (1994) suggests that the calculated partition coefficient values may increase with decreasing Cu content of the mss and additionally, increase with increasing fS_2 of the system.

The absolute magnitude of the depletion of Pt and Pd from the silicate melt phase ultimately depends on the fS_2 of the magmatic system, as the stability field for mss at magmatic conditions spans nearly 10 orders of magnitude. Thus, it is conceivable that a silicate melt could precipitate mss, yet retain significantly less Pt and Pd than are soluble in mss at much higher fS_2, significantly lowering the apparent partition coefficient values. Similarly, mss saturation may be inhibited entirely given the appropriate fO_2, fS_2 and fH_2O conditions. Hydrous silicate melts containing dissolved S at a fixed fO_2 and fH_2O will posses a defined and fixed fH_2S, given the appropriate low magmatic fO_2. Sulfidation reactions involving ferrous iron dissolved in the silicate melt or the transformation of mt to mss may be described by the following equilibria:

$$FeO^{melt} + H_2S = FeS^{mss} + H_2O \quad (12)$$

$$1/3Fe_3O_4 + H_2S = FeS^{mss} + H_2O + 1/6O_2 \quad (13)$$

Assuming the mss in Eqs. (8) and (9) and mt in Eq. (9) are pure phases, these reactions work in concert with the iron activity in the melt, fS_2 and fO_2 to buffer the fugacity of the gaseous species H_2S and H_2O in the melt.

$$K_8 = \frac{f_{H_2O}}{X_{FeO}^{melt} \cdot f_{H_2S}} \cdot (\gamma_{FeO}^{melt})^{-1} \quad (14)$$

where X_{FeO}^{melt} is the mole fraction of dissolved FeO in the silicate melt, f_{H_2O} is the fugacity of water, f_{H_2S} is the fugacity of H_2S, and γ_{FeO}^{melt} is the activity of FeO in the melt. The f_{H_2O} is related to f_{O_2} and f_{H_2S} via the equilibrium:

$$K_9 = \frac{fH_2O \cdot fO_2^{1/6}}{fH_2S} \quad (15)$$

If the intrinsic values of fH_2O and fH_2S fixed by the water content, sulfur content and oxidation state of the melt are out of equilibrium with the buffered values required by Eqs. (8) and (9), mss will be either resorbed and consumed until it is exhausted, or crystallize until the ratio of fH_2S and fH_2O of the silicate melt reach the equilibrium buffered values. Alternatively in sulfide unsaturated systems, high fH_2O values may impede entirely the crystallization of a sulfide phase given that the melt is sufficiently oxidized (i.e., at oxidation states where H_2S formation is limited, as reduced melts with high fH_2O will have a high propensity to crystallize an oxide phase). The "instantaneous" water fugacity of the melt at any point during magmatic evolution (prior to vapor saturation by second boiling) exerts a first order control on the stability and modal abundance of crystalline mss present in the system. The reduction in a_{FeS}^{mss} by the incorporation of additional metal components (i.e., Cu, Ni and Co) into the mss lattice will shift the pure end member equilibrium dictated by Eqs. (8) and (9) in a direction that represses mt crystallization.

The model equilibria discussed above indicate that early saturation of a silicate melt with mss (given an appropriately high fS_2), provided that the mss is removed from the system via a Rayleigh type fraction process, may effectively reduce the PGE budget of the system levels that preclude the development of a PGE rich porphyry system. However, mss saturation at low fS_2 values may be possible given a high a_{FeO}^{melt} and appropriate fO_2, fH_2O and fH_2S. Under such low fS_2 conditions, the ability of mss to deplete the melt of Pt and Pd should be drastically reduced relative to high fS_2 conditions. Additionally, at low fS_2 conditions conducive to the saturation of a magmatic sulfide phase the modal abundance of crystalline mss should be extremely low due to the low concentrations of *S* acting as a limiting reagent.

4.1.2. The effect of iss saturation

Crystallization of iss also appears to fractionate Pt, Pd and Au in the silicate melt. The effect of iss crystallization is to fractionate Au and Pd from Pt in the silicate melt with Pt being retained most strongly in the melt phase. Gold and Pd concentrations in iss range from 1000 to 5000 μg/g, whereas the concentration of Pt in iss is consistently below the EPMA limit of detection. It is interesting to note the similarity of the geochemical behavior of Pd and Au in iss when contrasted with the distinctly, dissimilar behavior of these metals in recovered mss. There appears to be no systematic variation of the Pt, Pd or Au solubility in iss with variation in either fS_2 or the Fe/Cu ratio of the recovered iss. Gold concentrations reported in this study are similar to, albeit larger, than those reported in Simon et al. (2000). The fractionation trend of Pt and Pd, induced by the stability of magmatic iss, mirrors the mss fractionation trend where the concentration of Pt in the silicate melt exceeds that of Pd. The relatively compatible behavior of Au in iss differs distinctly from that observed in mss at the same experimental conditions. The compatible behavior of Au in the iss lattice should result in an inverse fractionation effect with respect to the ratio of Au to Pt and Pd in the residual silicate melt. Such a situation should strip Au from the melt relative to Pd and Pt.

5. APPLICATION TO NATURAL SYSTEMS

The observed fractionation trends induced by the crystallization of mss with respect to the metal content of the residual melt are not in agreement with the high Pt/Pd ratios observed in some porphyry ore systems (Auge et al., 2005). The discord between Pt/Pd ratios observed in PGE-rich porphyry ore deposits (Werle et al., 1984; Mutschler et al., 1985; Hulbert et al., 1988), Mulja and Mitchell, 1991; Cassidy et al., 1996; Ohnenstetter and Watkinson, 1998) and the Pt/Pd ratios caused by sulfide saturation, as constrained in this study, suggest that magma oxidation and subsequent sulfide resorption and/or chemical exchange of metallic species between crystalline magmatic sulfide material and an evolved aqueous magmatic fluid play dominant roles in the determination of the final Pt/Pd ratio of the ore system. Furthermore, sulfide saturation early in the evolution of a rhyolite silicate magma and the subsequent removal of the sulfide phase via Rayleigh fractionation may reduce the concentrations of Pt and Pd in the silicate melt to levels too low for the PGE to be effectively scavenged and concentrated by a magmatic volatile phase in porphyry ore-forming systems.

6. CONCLUDING REMARKS

Our experimental results constrain fractionation trends amongst Pd, Pt and Au in rhyolite magmatic systems. The data suggest that the timing of sulfide saturation and the nature of magmatic sulfide phase stability may control the ultimate abundances and ratios of Pd, Pt and Au transported by magmatic hydrothermal fluids to porphyry-type ore forming systems. Early crystallization of a magmatic sulfide phase in an evolving rhyolite melt system (and the removal of this phase from further chemical interaction with the rest of the magmatic system) may effectively stifle volatile-phase transport of the PGE and their enrichment in the magmatic-hydrothermal environment with metal ratios consistent with those observed in nature. Magmatic sulfide phases may, however, play an important temporal role in liberating sequestered Pt and Pd via oxidation and resorbtion into the melt or via direct sulfide–aqueous fluid chemical interaction late in the magmatic-hydrothermal transition phase.

ACKNOWLEDGMENTS

This work was supported by the National Science Foundation NSF EAR 0609550. We thank Ed Mathez, Chusi Li and an anonymous reviewer for comments that significantly improved the manuscript, both substantively and stylistically; also James Brenan and Thomas Pettke are thanked for informal reviews. We thank Wohlgemuth-Ueberwasser and Chris Ballhuas for providing sulfide standards for LA-ICP-MS analyses, Dave London for providing the starting glass, and George Harlow for the starting bn, cp and po. AB thanks the Society of Economic Geology, Geological Association of Canada/Mineralogical Association of Canada, the UNLV Department of Geoscience and the UNLV Graduate and Professional Student Association.

REFERENCES

Auge T. M., Petrunov R. and Bailly L. (2005) On the origin of the PGE mineralization in the elatsite porphyry Cu–Au deposit, Bulgaria: comparison with the Baula–Nuasahi complex, India, and other alkaline PGE-rich porphyries. *Can. Mineral.* **43**, 1352–1375.

Ballhaus C. and Ulmer P. (1995) Platinum-group elements in the Merensky reef: II. Experimental solubilities of platinum and palladium in Fe1-xS from 950 to 450 °C under controlled fS2 and fH2. *Geochim. Cosmochim. Acta* **59**, 4881–4888.

Blaine F. A., Linnen R. L., Holtz F. and Brügmann G. E. (2005) Platinum solubility in a haplobasaltic melt at 1250 °C and 0.2 GPa: the effect of water content and oxygen fugacity. *Geochim. Cosmochim. Acta* **69**, 1265–1273.

Bodnar R. J., Burnham C. W. and Sterner S. M. (1985) Synthetic fluid inclusions in natural quartz. III. Determination of phase equilibrium properties in the system H_2O–NaCl to 1000 °C and 1500 bars. *Geochim. Cosmochim. Acta* **49**, 1861–1873.

Borisov A. and Palme H. (1997) Experimental determination of the solubility of platinum in silicate melts. *Geochim. Cosmochim. Acta* **61**, 4349–4357.

Candela P. A. (1991) Physics of aqueous phase exsolution in plutonic environments. *American Mineralogist* **76**, 1081–1091.

Carroll M. R. and Rutherford M. J. (1988) Sulfur speciation in hydrous experimental glasses of varying oxidation states. Results from measured wavelength shifts of sulfur X-rays. *Am. Mineral.* **73**, 845–849.

Cassidy K. F., Lang, Jr., Lueck, B. A., Mortensen J. K., Russel J. K., Thompson J. F. H. (1996). Geochemical and isotopic characteristics of Mesozoic alkalic intrusions in the Cordillera nf British Columbia: tectonic significance and implications for Cu–Au metallogeny. *Geol. Soc. Austral.*, 13th Australian *Geological Convection*, Canberra, February, 1996. #41 (abstr.).

Chou I.-M. (1987). Oxygen buffer hydrogen sensor techniques at elevated pressures and temperatures. In *Hydrothermal Experimental Techniques* (eds. G. C. Ulmer and H. L. Barnes), pp. 61–99.

Chou I.-M., Sterner S. M. and Pitzer K. S. (1992) Phase relations in the system NaCl KCl–H_2O: IV. Differential thermal analysis of the sylvite liquidus in the KCl–H_2O binary, the liquidus in the NaCl–KCl–H_2O ternary, and the solidus in the NaCl–KCl binary to 2 kb pressure, and a summary of experimental data for thermodynamic-PTX analysis of solid–liquid equilibria at elevated P–T conditions. *Geochim. Cosmochim. Acta* **56**, 2281–2293.

Clemente B., Scaillet B. and Pichavant M. (2004) The solubility of sulphur in rhyolitic melts. *J. Petrol.* **45**, 2171–2196.

Cottrell E. and Walker D. (2006) Constraints on core formation from Pt partitioning in mafic silicate liquids at high temperatures. *Geochim. Cosmochim. Acta* **70**, 1565–1580.

Dixon J. E., Clague D. A. and Stolper E. M. (1991) Degassing history of water, sulfur, and carbon in submarine lavas from Kilauea Volcano, Hawaii. *J. Geol.* **99**, 371–394.

Ertel W., O'Neill H., Sylvester P. J. and Dingwell D. B. (1999) Solubilities of Pt and Rh in a haplobasaltic silicate melt at 1300 °C. *Geochim. Cosmochim. Acta* **63**, 2439–2449.

Farges F., Neuville D. R. and Brown G. E. (1999) Structural investigation of platinum solubility in silicate glasses. *Am. Miner.* **84**, 1562–1568.

Fleet M. E., Crocket J. H. and Stone W. E. (1991) Partitioning of palladium, iridium, and platinum between sulfide liquid and basalt melt: effects of melt composition, concentration, and oxygen fugacity. *Geochim. Cosmochim. Acta* **55**, 2545–2554.

Fleet M. E., Crocket J. H., Liu M. and Stone W. E. (1999) Laboratory partitioning of platinum-group elements (PGE) and gold with application to magmatic sulfide-PGE deposits. *Lithos* **47**, 127–142.

Frank M. R., Candela P. A., Piccoli P. M. and Glascock M. D. (2002) Gold solubility, speciation, and partitioning as a function of HCl in the brine-silicate melt-metallic gold system at 800 °C and 100 MPa. *Geochim. Cosmochim. Acta* **66**, 3719–3732.

Guillong M., Meier D. M., Allan M. M., Heinrich C. A. and Yardley B. (2008) *SILLS: A MATLAB-Based Program for the Reduction of Laser Ablation ICP–MS Data of Homogeneous Materials and Inclusions: Mineralogical Association of Canada Short Course 40*. Vancouver, B.C., pp. 328–333.

Guillong M. and Heinrich C. A. (2007) Sensitivity enhancement in laser ablation ICP-MS using small amounts of hydrogen in the carrier gas. *J. Anal. Atomic Spectrom.* **22**, 1488–1494.

Holzheid A. and Lodders K. (2001) Solubility of copper in silicate melts as function of oxygen and sulfur fugacity, temperature, and silicate composition. *Geochim. Cosmochim. Acta* **65**, 1933–1951.

Hulbert L. J., Duke J. M., Eckstrand O. R., Lydon J. W. and Scoates R. F. J. (1988) Geological environments of the platinum group elements. *Geol. Surv. Canada Open File 1440*, 148.

Jugo P. J., Candela P. A. and Piccoli P. M. (1999) Magmatic sulfides and Au:Cu ratios in porphyry deposits: an experimental study of copper and gold partitioning at 850 °C, 100 MPa in a haplogranitic melt-po-intermediate solid solution-gold metal assemblage, at gas saturation. *Lithos* **46**, 573–589.

Li C., Ripley E. M. and Mathez E. A. (2003) The effect of S on the partitioning of Ni between olivine and silicate melt in MORB. *Chemical Geol.* **201**, 295–306.

Lynton S. J., Candela P. A. and Piccoli P. M. (1993) An experimental study of the partitioning of copper between pyrrhotite and a high silica rhyolitic melt. *Econ. Geol.* **88**, 901–915.

McMillan P. and Holloway J. (1987) Water solubility in aluminosilicate melts. *Contrib. Mineral. Petrol.* **97**, 320–332.

Morgan G. B. and London, VI, D. (1996) Optimizing the electron microprobe analysis of hydrous alkali aluminosilicate glasses. *Am. Mineral.* **81**, 1176–1185.

Mulja T. and Mitchell R. H. (1991) The Geordie Lake intrusion, Coldwell complex, Ontario: a palladium- and tellurium-rich disseminated sulphide occurrence derived from an evolved tholeiitic magma. *Econ. Geol.* **86**, 1050–1069.

Mutschler F. E., Griffin M. E., Scott S. D. and Shannon S. S. (1985) Precious metal deposits related to alkaline rocks in the North American Dordillera – an interpretative review. *Trans. Geol. Soc. S. Africa* **88**, 355–377.

Ohnenstetter D. and Watkinson D. H. (1998) Low-temperature evolution of the platinum group mineralogy, Two Duck Lake intrusions, Coldwell Complex, Ontario, Canada. In *International Platinum 1998* (eds. N. P. Laveroux and V. V. Dislter). Theophrastus Publishing, St. Petersburg, pp. 116–118.

O'Neill H. St. C. and Mavrogenes J. A. (2002) The sulfide capacity and the sulfur content at sulfide saturation of silicate melts at 1400 °C and 1 bar. *J. Petrol.* **43**, 1049–1087.

Peach C. L., Mathez E. A. and Keays R. R. (1990) Sulfide–silicate melt distribution coefficients for noble metals and other chalcophile elements as deduced from MORB implications for partial melting. *Geochim. Cosmochim. Acta* **54**, 3379–3389.

Scaillet B. and MacDonald R. (2001) Phase reations of peralkaline silicic magmas and petrogenetic implications. *J. Petrol.* **42**, 825–845.

Simon G., Kesler S. E. and Essene E. J. (2000) Gold in porphyry copper deposits: experimental determination of the distribution

of gold in the Cu–Fe–S system at 400 to 700 °C. *Econ. Geol.* **95**, 259–270.

Simon A. C., Pettke T., Candela P. A., Piccoli P. M. and Heinrich C. A. (2005) Gold partitioning in melt–vapor–brine systems. *Geochim. Cosmochim. Acta* **69**(332), 1–3335.

Simon A. C., Pettke T., Candela P. A., Piccoli P. M. and Heinrich C. (2006) Copper partitioning in sulfur bearing magmatic systems. *Geochim. Cosmochim. Acta* **70**, 5583–5600.

Simon A. C., Pettke T., Candela P. A., Piccoli P. M. and Heinrich C. (2007) The partitioning behavior of As and Au in a haplogranite – vapor at magmatic conditions in sulfur-free and sulfur-bearing systems. *Geochim. Cosmochim. Acta* **71**, 1764–1782.

Simon A. C., Pettke T., Candela P. A., Piccoli P. M. and Heinrich C. (2008) The partitioning behavior of silver in a vapor–brine–rhyolite melt assemblage. *Geochim. Cosmochim. Acta* **72**, 1638–1659.

Stone W. E., Crocket J. H. and Fleet M. E. (1990) Partitioning of palladium, iridium, platinum, and gold between sulfide liquid and basalt melt at 1200 °C. *Geochim. Cosmochim. Acta* **54**, 2341–2344.

Toulmin P. and Barton P. B. (1964) A thermodynamic study of pyrite and pyrrhotite. *Geochim. Cosmochim. Acta* **64**, 641–671.

Tsujimura T. and Kitakaze A. (2004) New phase relations in the Cu–Fe–S system at 800 °C; constraint of fractional crystallization of a sulfide liquid. *Neues Jahrbuch für Mineralogie Monatshefte* **10**, 433–444.

Ripley E. M., Brophy J. G. and Li C. (2002) Copper solubility in a basaltic melt and sulfide liquid/silicate melt partition coefficients of Cu and Fe. *Geochim. Cosmochim. Acta* **66**, 2791–2800.

Rudnick R. L. and Gao S. (2003) The composition of the continental crust. In *The Crust*, Treatise on Geochemistry (ed. R. L. Rudnick), pp. 1–64. vol. 3. Elsevier-Pergamon, Oxford.

Wallace P. and Carmichael I. S. E. (1992) Sulfur in basaltic magmas. *Geochim. Cosmochim. Acta* **56**, 1683–1874.

Werle J. L., Ikramuddin M. and Mutschler M. E. (1984) Allard Stock, La Plata Mountains, Colorado—an alkaline rock-hosted porphyry copper—precious metal deposit. *Can. J. Earth Sci.* **21**, 630–641.

Witter J. B., Kress V. C. and Newhall C. G. (2005) Volcán Popocatépetl, Mexico: Petrology, magma mixing, and immediate sources of volatiles for the 1994–present eruption. *J. Petrol.* **46**, 2337–2366.

Wohlgemuth-Ueberwasser C. C., Ballhaus C., Berndt J., Stotter nee Paliulionyte V. and Meisel T. (2007) Synthesis of PGE sulfide standards for laser ablation inductively coupled plasma mass spectrometry (LA-ICP-MS). *Contrib. Mineral. Petrol.* **154**, 607–617.

Associate editor: Edward M. Ripley